

Thermal and Non-thermal X-Rays from the Galactic Supernova Remnant G348.5+0.1

Shigeo YAMAUCHI, Sari MINAMI, and Naomi OTA,

Department of Physics, Faculty of Science, Nara Women's University, Kitauoyanishi-machi, Nara 630-8506
yamauchi@cc.nara-wu.ac.jp

and

Katsuji KOYAMA

Department of Physics, Graduate School of Science, Kyoto University, Kitashirakawa-Oiwake-cho, Sakyo-ku, Kyoto 606-8502
Department of Earth and Space Science, Graduate School of Science, Osaka University,
1-1 Machikaneyama-cho, Toyonaka, Osaka 560-0043

(Received ; accepted)

Abstract

We report on Suzaku results of the two distinct regions in the Galactic supernova remnant G348.5+0.1: extended thermal X-rays ("soft diffuse") at the northeast region and non-thermal X-rays (CXOU J171419.8–383023) at the northwest region. The X-ray spectrum of the soft diffuse is fitted with neither an ionization equilibrium nor a non-equilibrium (ionizing) plasma model, leaving saw-teeth residuals in the 1.5–3 keV energy band. The residual structures can be produced when free electrons are recombined to the K-shells of highly ionized Mg and Si ions. In fact, the X-ray spectrum is nicely fitted with a recombination-dominant plasma model. We propose a scenario that the plasma in nearly full ionized state at high temperature quickly changed to a recombining phase due to selective cooling of electrons to a lower temperature of ~ 0.5 keV. The spectrum of CXOU J171419.8–383023 is well explained by a simple power-law model with a photon index of 1.9, nearly equal to the typical value of pulsar wind nebulae. Since the distance is estimated to be the same as that of the soft diffuse, we infer that both the soft diffuse and CXOU J171419.8–383023 are associated with the same object, SNR G348.5+0.1.

Key words: ISM: individual (G348.5+0.1) — ISM: supernova remnants — X-rays: ISM — X-rays: spectra

1. Introduction

G348.5+0.1 (CTB 37A) is a supernova remnant (SNR) discovered in the radio band (Clark et al. 1975). The radio image shows a shell-like structure at the north and a break-out morphology extending to the south. The radio angular size and the spectral index are $15'$ and 0.3, respectively (Green 2009 and references therein). Around this SNR, CO molecular clouds were found (Reynoso & Mangum 2000) and OH masers were discovered in the molecular clouds (Frail et al. 1996; Reynoso & Mangum 2000). These suggest interactions of the SNR shock with the surrounding molecular clouds. The distance was estimated to be 11.3 kpc (Reynoso & Mangum 2000) or 6.3–9.5 kpc (Tian & Leahy 2012).

X-ray emission from G348.5+0.1 was first discovered in the ASCA Galactic Plane Survey (Yamauchi et al. 2002, 2008). The X-rays with a large absorption column of interstellar matter are located within the radio shell (Yamauchi et al. 2008). Aharonian et al. (2008) reported Chandra and XMM-Newton results that G348.5+0.1 consists of two components; one is an extended thermal X-ray emission at the northeast part (here "soft diffuse") and the other is a non-thermal X-ray source with a small extent at the northwest part, named as CXOU J171419.8–383023. The Suzaku spectrum of the soft diffuse was fitted with

a two-component model, a collisional ionization equilibrium (CIE) plasma with a temperature of 0.63 keV and a solar abundance and a power-law component with a photon index of 1.6 (Sezer et al. 2011). Based on the spatial and spectral properties, a center-filled thermal X-ray emission within the radio shell, Sezer et al. (2011) noted that G348.5+0.1 is a new member of mixed-morphology (MM) SNRs.

Aharonian et al. (2008) discovered very high energy γ -rays (VHE- γ) at the position of G348.5+0.1 with High Energy Stereoscopic System (H.E.S.S.), named as HESS J1714–385. The spatial distribution of the VHE- γ is consistent with that of the molecular clouds. At the northeast part of the SNR, GeV γ -rays were found with the Fermi Large Area Telescope (LAT) (Castro & Slane 2010).

The X-ray spectra of most of the MM SNRs have been well explained with a thermal plasma in either an ionization equilibrium or an ionizing phase. Recently, on the other hand, a recombination-dominant plasma (RP) have been discovered from six MM SNRs (Yamaguchi et al. 2009; Ozawa et al. 2009; Ohnishi et al. 2011; Sawada & Koyama 2012; Uchida et al. 2012; Yamauchi et al. 2013). These SNRs share some common characteristics; all are accompanied with OH masers in surrounding molecular clouds and most of them are either GeV or TeV γ -ray sources.

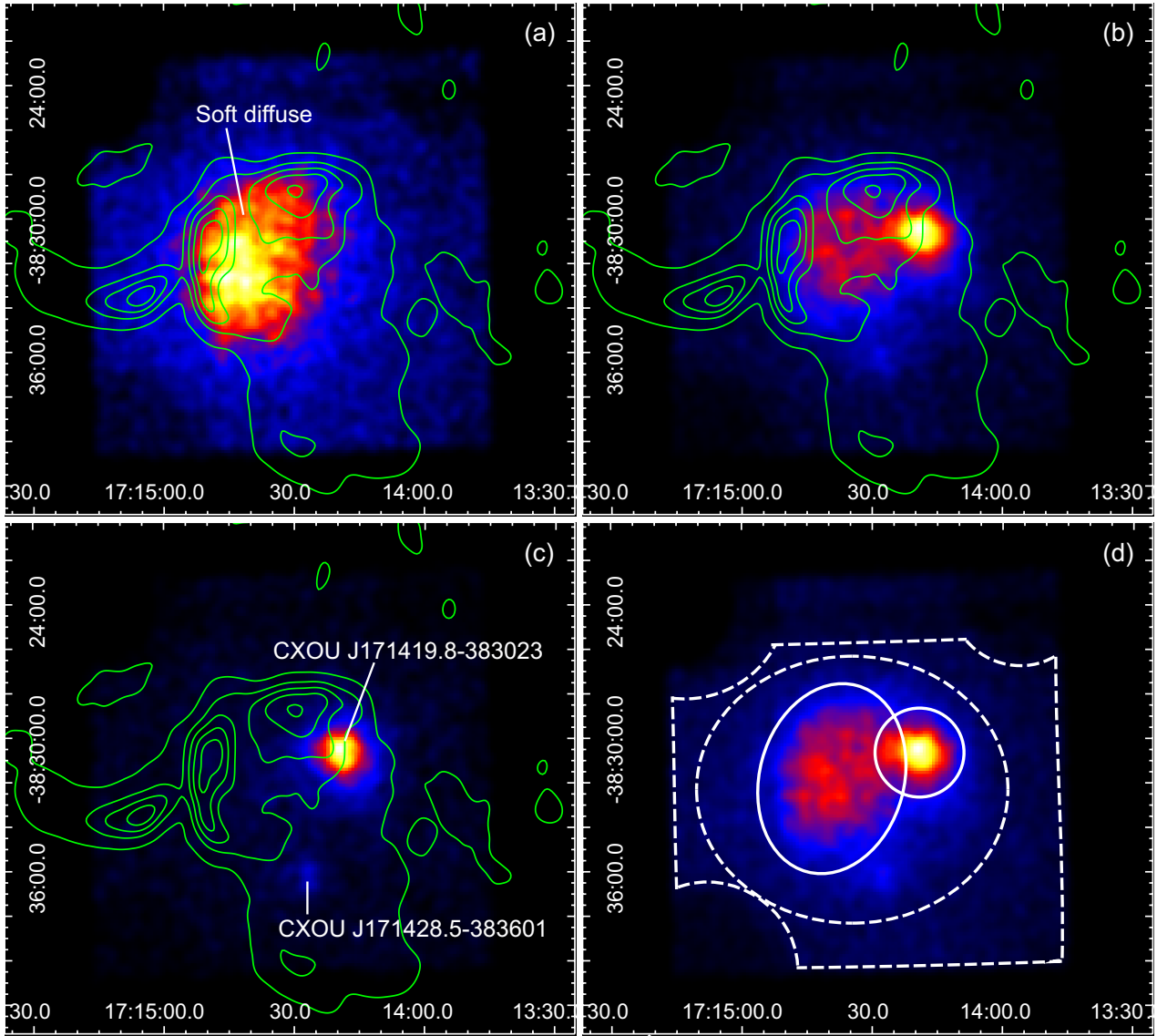


Fig. 1. XIS images of G348.5+0.1 in the 0.7–2 (a), 2–5 (b), 5–8 (c), and 0.7–8 keV (d) energy bands (color). The coordinates are J2000.0. The radio map at 843 MHz using the Molonglo Observatory Synthesis Telescope (MOST) is displayed by the green contours in (a)–(c) (Whiteoak & Green 1996). The X-ray images from XIS0, 1, and 3 were co-added, but neither the background subtraction nor the vignetting correction was made. The images were smoothed with a Gaussian distribution with the kernel of $\sigma=24''$. The intensity levels of the X-ray and radio bands are linearly spaced. The solid ellipse and circle in (d) show the source regions for the soft diffuse and CXOU J171419.8–383023, respectively, while the background region is also shown by the dashed line in (d).

Although G348.5+0.1 shows the same characteristics, no RP has been reported so far (e.g., Aharonian et al. 2008; Sezer et al. 2011), possibly due to limited statistics (Aharonian et al. 2008) or improper estimate of the large background in the Galactic ridge region (Sezer et al. 2011). Since Suzaku has the best performance for the spectral analysis of faint and diffuse sources, we reprocessed and reanalyzed the Suzaku data paying particular concern to background subtraction and a model fitting procedure. We found new results of possible evidence for the RP in the soft diffuse of the MM SNR G348.5+0.1 and the most accurate value for physical parameters of the soft diffuse and CXOU J171419.8–383023. In this paper, we report new revised results of the X-ray spectra and discuss the nature of G348.5+0.1. Throughout this paper, the quoted errors are at the 90% confidence level.

2. Observation and Data Reduction

Systematic survey observations studying various MM-SNRs on the Galactic plane were carried out with the Suzaku satellite (Mitsuda et al. 2007). G348.5+0.1 was observed on 2010 February 20–21 (Obs. ID 504097010) with the CCD cameras (XIS, Koyama et al. 2007) placed at the focal planes of the thin foil X-ray Telescopes (XRT, Serlemitsos et al. 2007). The pointing position was $(l, b)=(348^\circ44, +0^\circ09)$.

XIS sensor-1 (XIS1) is a back-side illuminated (BI) CCD, while XIS sensor-0, 2, and 3 (XIS0, 2, and 3) are front-side illuminated (FI) CCDs. The Field of view (FOV) of the XIS is $17'.8 \times 17'.8$. Since XIS2 turned dysfunctional in 2006 November¹, we used the data obtained with the other CCD cameras (XIS0, 1, and 3). A small fraction of the XIS0 area was not used, because of the data damage due possibly to an impact of micro-meteorite on 2009 June 23². The XIS was operated in the normal clocking mode. The spectral resolution of the XIS was degraded due to the radiation of cosmic particles 4.5 years after the launch. It was restored by the spaced-row charge injection (SCI) technique. Details of the SCI technique are given in Nakajima et al. (2008) and Uchiyama et al. (2009).

Data reduction and analysis were made with the HEASoft version 6.12 and SPEX (Kaastra et al. 1996) version 2.02.04. The XIS pulse-height data for each X-ray event were converted to Pulse Invariant (PI) channels using the `xispi` software and the calibration database version 2012-07-03. We rejected the data taken at the South Atlantic Anomaly, during the earth occultation, and at the low elevation angle from the earth rim of $< 5^\circ$ (night earth) and $< 20^\circ$ (day earth). The exposure time after these screenings was 53.8 ks.

3. Analysis and Results

3.1. X-Ray Image

Figure 1 shows X-ray images of G348.5+0.1 in the 0.7–2, 2–5, 5–8, and 0.7–8 keV energy bands. To maximize

¹ <http://www.astro.isas.jaxa.jp/suzaku/news/2006/1123/>

² <http://www.astro.isas.jaxa.jp/suzaku/news/2009/0702/>

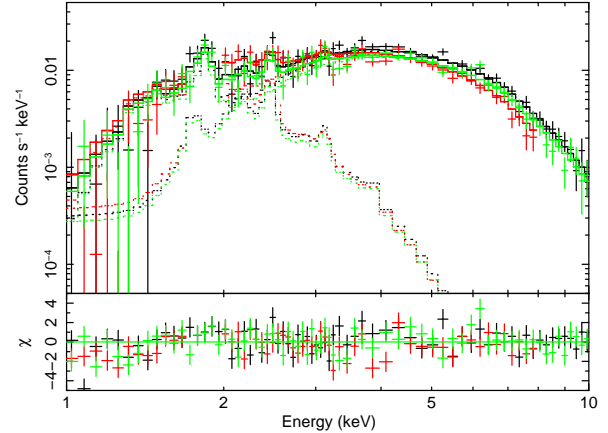


Fig. 2. Upper: X-ray spectra of the CXOU J171419.8–383023 region (XIS0: black, XIS1: red, and XIS3: green) and the best-fit model. Lower: residuals from the best-fit model.

Table 1. The best-fit parameters of CXOU J171419.8–383023 derived from a combined spectral analysis.

Parameter	Value
N_{H} ($\times 10^{22}$ cm $^{-2}$)	$7.6^{+1.1}_{-1.0}$
Photon index	$1.94^{+0.15}_{-0.14}$

the photon statistics, the data of XIS0, 1, and 3 were combined. We confirmed that the X-ray emission is located at the north part and found no significant X-ray emission in the break-out radio morphology extending to the south.

In the soft X-ray band (0.7–2 keV), diffuse X-rays are clearly seen at the northeast part of the SNR (soft diffuse). On the other hand, we see a compact source at the northwest part in the hard X-ray band (CXOU J171419.8–383023, Aharonian et al. 2008). In addition to the soft diffuse and CXOU J171419.8–383023, another hard X-ray source was found at the south. It is identified with CXOU J171428.5–383601 (Aharonian et al. 2008).

3.2. X-Ray Spectra

In order to collect X-ray photons from the soft diffuse and CXOU J171419.8–383023 as many as possible, we extracted X-ray spectra from the partially overlapping two regions. The solid ellipse and circle in figure 1d show the source regions for the soft diffuse and CXOU J171419.8–383023, respectively. The background data were taken from a source free region in the same FOV as large as possible, which is shown by the dashed area in figure 1d. In order to estimate the background counts in the source region carefully, we should take account of the difference of vignetting effects between the source and background regions. We made background-subtracted spectra by the following procedure as described in Hyodo et al.

(2008).

(1) We constructed the non-X-ray background (NXB) for the source and the background spectra from the night earth data using `xisnxbgen` (Tawa et al. 2008) and then subtracted the NXB from the source and the background spectra.

(2) The vignetting effect of the background spectrum was corrected by multiplying the effective area ratios between the source and the background regions for each energy bin.

(3) Then, we subtracted the vignetting-corrected background data from the source region data.

Fractions of the background counts in the 1–8 keV band were 25–27% and 18–22% for the soft diffuse and the CXOU J171419.8–383023 region data, respectively. Redistribution Matrix Files (RMFs) were made using `xisrmfgen`, while Ancillary Response Files (ARFs), were simulated using a Chandra image for the photon distribution data in `xissimarfgen`. The XIS0, 1 and 3 spectra were simultaneously fitted. Since the XIS gain calibration is known to be problematic around the Si K-edge energy, we ignored the XIS1 data in the energy of 1.75–1.95 keV.

As we can see in figure 1d, the spectra extracted from the CXOU J171419.8–383023 region include some fraction of the soft diffuse X-rays, and vice versa. We therefore carried out combined fitting using a two-component model consisting of a thermal plasma (TP) and a power-law (PL) function. These models are based on the spatially resolved analysis with Chandra and XMM-Newton; the soft diffuse is fitted with a TP model, while CXOU J171419.8–383023 is fitted with a PL model (Aharonian et al. 2008, see also Sezer et al. 2011). In the combined fitting, we assume the spectral shape of the TP and PL models are the same between the soft diffuse and the CXOU J171419.8–383023 regions.

Comparing the Suzaku X-ray image with the CO map (Reynoso & Mangum 2000), we found that the CO cloud covers the CXOU J171419.8–383023 region but does not cover the most part of the soft diffuse region. We hence applied independent absorptions (N_{H}) for the TP and the PL components. The applied model is

$$\text{Absorption1} \times \text{TP} + \text{Absorption2} \times \text{PL}.$$

Here, we used a CIE (`vappec` in `xspec`) model as a TP model. The cross sections of photoelectric absorption were taken from Morrison and McCammon (1983) and the abundance tables were taken from Anders and Grevesse (1989). The abundances of Mg, Si, S, and Ar were free parameters, while those of Al and Ca were assumed to be the same as Mg and Ar, respectively. The other elements were fixed to the solar abundances. Both the spectra of CXOU J171419.8–383023 and the soft diffuse regions were reasonably represented by this combined model with $\chi^2/\text{d.o.f.} = 549/428$. The best-fit two-component model and the best-fit parameters of the PL model for CXOU J171419.8–383023 are shown in figure 2 and table 1, respectively. As a TP contamination from the soft diffuse, we used a CIE model. However, as we reveal in the following paragraphs, a CIE model does not exactly repre-

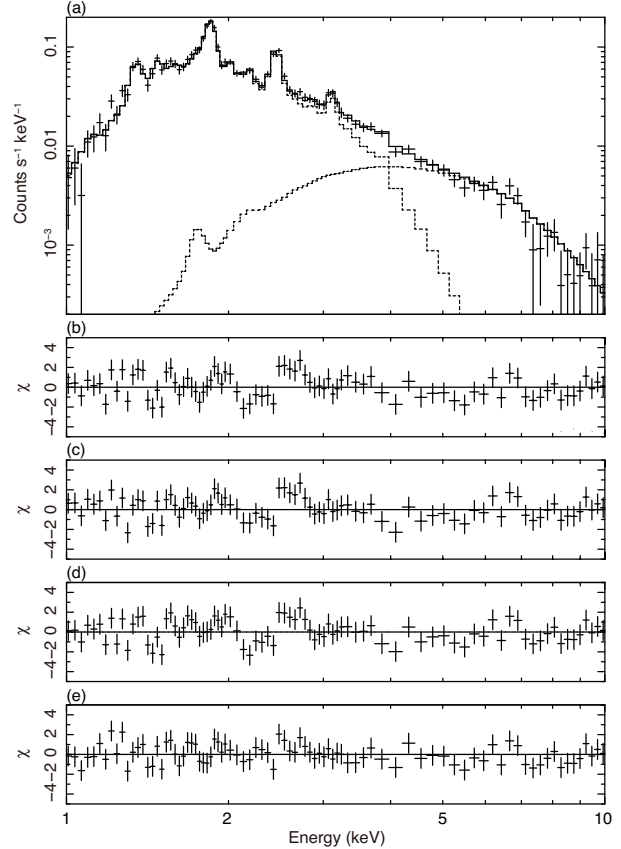


Fig. 3. X-ray spectra (XIS0+XIS3) of the soft diffuse region and the residuals from the best-fit model. The histogram in (a) is the best-fit RP+PL model, while the residuals from the models of CIE+PL, 2CIE+PL, IP+PL, and RP+PL are shown in (b), (c), (d) and (e), respectively (see table 2)

sent the spectra of the soft diffuse (see figure 3 and table 2). We therefore re-fitted the spectra from the CXOU J171419.8–383023 region with the PL model fixing the best-fit TP model given in table 2, and obtained the consistent PL parameters with those given in table 1.

For the soft diffuse spectra, we see significant residuals from the two-component model. We therefore examined the soft diffuse spectra using several TP models fixing the spectral parameters of the PL model (photon index and N_{H} value) to the best-fit values in table 1. At first, a CIE (`vappec` in `xspec`) model was examined, but was rejected with χ^2 value of 285 (d.o.f.=236). The best-fit parameters are listed in table 2, while the residuals are plotted in figure 3b. Although the fitting was simultaneously made for XIS0, XIS1 and XIS3, we show the co-added (XIS0+XIS3) results in figure 3. The best-fit thermal plasma parameters are consistent with those in Sezer et al. (2011). We, however, found clear residuals (saw-teeth structures) in the 1.5–3 keV energy band, $\sim 10\text{--}40\%$ excess above the model. This excess is larger than the systematic error of the effective area in this energy band estimated from the Crab spectra ($< 5\%$)³, and hence the saw-teeth residuals

³ <http://www.astro.isas.jaxa.jp/suzaku/doc/suzakumemo/suzakumemo->

Table 2. The best-fit parameters derived from a spectral analysis for the soft diffuse region.

Parameter	Value			
Model	CIE+PL	2 CIE+PL	IP+PL	RP+PL
	XSPEC: vapec	XSPEC: 2 vapec	SPEX: neij	SPEX: neij
N_{H} ($\times 10^{22}$ cm $^{-2}$)	$3.6^{+0.1}_{-0.2}$	$4.1^{+0.4}_{-0.2}$	3.5 ± 0.2	3.5 ± 0.2
kT_{e} [initial] (keV)	—	—	0.001 (fixed)	5 (fixed)
kT_{e} (keV)	$0.63^{+0.03}_{-0.02}$	$0.70^{+0.03}_{-0.05}$	$0.67^{+0.06}_{-0.04}$	$0.49^{+0.09}_{-0.06}$
$n_{\text{e}}t^*$ ($\times 10^{12}$ cm $^{-3}$ s)	—	—	$0.6^{+0.8}_{-0.3}$	$1.3^{+0.3}_{-0.1}$
Mg † = Al †	1.1 ± 0.2	$1.1^{+0.4}_{-0.3}$	$1.1^{+0.4}_{-0.3}$	1.2 ± 0.4
Si †	$1.0^{+0.1}_{-0.2}$	$1.3^{+0.2}_{-0.2}$	$1.3^{+0.2}_{-0.3}$	1.6 ± 0.3
S †	$1.1^{+0.1}_{-0.2}$	$1.1^{+0.2}_{-0.2}$	$1.2^{+0.2}_{-0.3}$	$1.7^{+0.3}_{-0.4}$
Ar † = Ca †	1.9 ± 0.5	$1.4^{+0.5}_{-0.4}$	1.6 ± 0.7	$3.1^{+1.3}_{-1.4}$
Others †	1 (fixed)	1 (fixed)	1 (fixed)	1 (fixed)
Power-law				
N_{H} ($\times 10^{22}$ cm $^{-2}$)	7.6 (fixed)	7.6 (fixed)	7.6 (fixed)	7.6 (fixed)
Photon index	1.94 (fixed)	1.94 (fixed)	1.94 (fixed)	1.94 (fixed)
$\chi^2/\text{d.o.f.}$	285/236	265/234	273/235	244/235

* Ionization or recombination timescale, where n_{e} is the electron density (cm $^{-3}$) and t is the elapsed time (s).

† Relative to the solar value (Anders & Grevesse 1989).

are not instrumental but real.

We also tried to fit the spectra with a two-temperature CIE model with the same abundances for the two CIE components. We found that the same structures remained in the residuals (the χ^2 value of 265 for d.o.f.=234, figure 3c).

We next examined a TP model in a non-equilibrium ionization (NEI) state (ionizing plasma: IP, **neij** in SPEX) with the assumption of an initial temperature of kT_{e} [initial]=0.001 keV. Then, we confirmed that the model also gave the large χ^2 value of 273 (d.o.f.=235) and the residuals were essentially the same as those of the CIE model (figure 3d). Since the leading edge energies of the saw-teeth structures at ~ 1.8 keV and ~ 2.4 keV correspond the K-shell ionization energies of the He-like Mg and Si, the residuals would be due to a radiative recombination continuum (RRC) which is a sign of the RP. Thus, we examined the RP model (**neij** in SPEX). This model gave a smaller χ^2 value than the IP model with $\Delta\chi^2 = 29$, but kT_{e} [initial] was not well constrained (kT_{e} [initial] > 1.6 keV). We then assumed kT_{e} [initial]=5 keV as a physically reasonable value and tried the final **neij** fitting. This model well represented the spectra with the χ^2 value of 244 (d.o.f.=235). The best-fit model and residuals are plotted in figure 3a and 3e, respectively. No systematic residual is seen in the 1.5–3 keV band. The best-fit parameters are listed in table 2.

4. Discussion

We reprocessed the Suzaku data of the Galactic SNR G348.5+0.1 paying particular concern to background subtraction. The reanalysis confirmed that G348.5+0.1 has two X-ray emission components, an extended soft X-ray emission at the northeast part dominant in the soft X-ray band (soft diffuse) and a hard X-ray source at the northwest part, CXOU J171419.8–383023. We further obtained new and accurate information on the X-ray emissions. In the following subsections, we discuss on the nature of the soft diffuse and CXOU J171419.8–383023.

4.1. Soft Diffuse Emission

The soft diffuse is located within the radio shell, and exhibited emission lines from highly ionized Mg, Si, S, Ar, and Ca, which clearly show that the X-ray emission is thermal origin. Thus, we confirm that G348.5+0.1 is a member of MM SNRs, as noted by Sezer et al. (2011). The model fits for the soft diffuse with a CIE, a 2 CIE or a standard NEI (ionizing) plasma model gave strong saw-teeth residuals in the 1.5–3 keV band, while a RP model well represented the overall spectra.

The column density of the hydrogen atom (N_{H_1}) along the line-of-sight to G348.5+0.1 is $(1.74\text{--}1.78) \times 10^{22}$ cm $^{-2}$ (Dickey & Lockman 1990) or $(1.29\text{--}1.43) \times 10^{22}$ cm $^{-2}$ (Kalberla et al. 2005). Using the mean value and the deviation, we estimate $N_{\text{H}_1} = (1.6 \pm 0.3) \times 10^{22}$ cm $^{-2}$. On the other hand, that of the hydrogen molecule (N_{H_2}) is estimated to be $(2.2 \pm 0.8) \times 10^{22}$ cm $^{-2}$ from the CO intensity (W_{CO}) around G348.5+0.1 of 87–157 K km s $^{-1}$

and the conversion factor from CO to H₂ ($N_{\text{H}_2}/W_{\text{CO}}$) of $(1.8 \pm 0.3) \times 10^{20} \text{ cm}^{-2} \text{ K}^{-1} \text{ km}^{-1} \text{ s}$ (Dame et al. 2001). Then, the total column density is estimated to be $N_{\text{H}} = N_{\text{H}_1} + 2N_{\text{H}_2} = (6.0 \pm 1.5) \times 10^{22} \text{ cm}^{-2}$. For the distance estimation of G348.5+0.1, we use the observed N_{H} of the soft diffuse because that of CXOU J171419.8–383023 may have additional absorption by the foreground molecular clouds. The best-fit value of $3.5 \times 10^{22} \text{ cm}^{-2}$ is 58% of the total column density along the line-of-sight to G348.5+0.1. If the line-of-sight length of the N_{H_1} and N_{H_2} estimation in the radio band is assumed to be 17 kpc, double the distance from the Sun to the Galactic center, the distance of G348.5+0.1 is estimated to be 9.9 ± 2.6 kpc. This value is consistent with those of the previous estimation (Reynoso & Mangum 2000; Tian & Leahy 2012). We therefore adopt the distance to be 10 kpc in the following discussion.

The size of the soft diffuse plasma is $\sim 8' \times 6'$ ($\sim 23.3 \text{ pc} \times 17.5 \text{ pc}$ at 10kpc). Dividing a radius of the major axis ($4' \sim 11.6 \text{ pc}$) by a sound velocity at a temperature of 0.49 keV, we can estimate a dynamical age of the SNR to be 2.4×10^4 year. Assuming that the line-of-sight length of the plasma is equal to the minor axis (the plasma shape is assumed to be an ellipsoid), the volume is estimated to be $1.1 \times 10^{59} f \text{ cm}^3$, where f is a filling factor. Adopting the best-fit volume emission measure of $8.9 \times 10^{58} \text{ cm}^{-3}$ and $n_e = 1.2n_{\text{H}}$, where n_e and n_{H} are the electron and hydrogen density, respectively, the mean hydrogen density is derived to be $n_{\text{H}} = 0.82 f^{-0.5} \text{ cm}^{-3}$. Then the recombination time ($n_e t / n_e$) is calculated to be $4.2 \times 10^4 f^{0.5}$ years, nearly the same as the dynamical age. We thus propose that the plasma was full ionized at high temperature ($> 1.6 \text{ keV}$) in the early phase of $4.2 \times 10^4 f^{0.5}$ years ago, and then the plasma changed to a recombining phase due to selective cooling of electrons to a lower temperature of $\sim 0.5 \text{ keV}$.

The RRC in the soft diffuse is weaker than those of the other RP-detected SNRs; the recombining timescale of the soft diffuse is $1.3_{-0.1}^{+0.3} \times 10^{12} \text{ cm}^{-3} \text{ s}$, while those of the other RP SNRs are $(0.1-0.7) \times 10^{12} \text{ cm}^{-3} \text{ s}$ (Sawada & Koyama 2012; Uchida et al. 2012; Yamaguchi et al. 2012; Yamauchi et al. 2013; S. Minami, private communication). Thus, the plasma in the soft diffuse of G348.5+0.1 would be the oldest among the RP SNRs.

4.2. CXOU J171419.8–383023

The spectrum of CXOU J171419.8–383023 is well explained by a simple PL model with a photon index of $1.94_{-0.14}^{+0.15}$ and a column density of $7.6_{-1.0}^{+1.1} \times 10^{22} \text{ cm}^{-2}$. These values are consistent with those with Chandra and XMM-Newton within the errors (Aharonian et al. 2008), but our values are more accurate with smaller errors.

The density of the northern cloud in the line-of-sight to CXOU J171419.8–383023 was reported to be $n_{\text{H}_2} = 660 \text{ cm}^{-3}$ (Reynoso & Mangum 2000). This corresponds to $N_{\text{H}} \sim 4 \times 10^{22} \text{ cm}^{-2}$, assuming the uniform density along the line-of-sight length of 10 pc (roughly equal to the width of the northern cloud). Since the best-fit N_{H} value of CXOU J171419.8–383023 is larger than that of the soft diffuse by $N_{\text{H}} = 4 \times 10^{22} \text{ cm}^{-2}$, it is likely that CXOU

J171419.8–383023 is at the same distance of the soft diffuse (10 kpc), and hence we infer that these two sources are physically associated with SNR G348.5+0.1. The unabsorbed X-ray flux of CXOU J171419.8–383023 in the 0.5–10 keV band is calculated to be $1.1 \times 10^{-11} \text{ erg s}^{-1} \text{ cm}^{-2}$ which roughly agrees with the Chandra/XMM-Newton results.

Aharonian et al. (2008) argued that CXOU J171419.8–383023 is a candidate for a pulsar wind nebula (PWN), although their best-fit photon index is smaller than those of typical PWNe. The weighted mean value of the photon index of 48 PWNe observed with Chandra is 2.01, in good agreement with our best-fit value, and hence CXOU J171419.8–383023 becomes a more likely candidate of PWN.

Possenti et al. (2002) and Mattana et al. (2009) presented the empirical relation between the X-ray luminosity and the characteristic age of pulsars in PWNe. Using the relation and the best-fit 2–10 keV band luminosity of $7 \times 10^{34} \text{ erg s}^{-1}$ at 10 kpc, we can estimate the age of CXOU J171419.8–383023 to be $\sim 10^3-10^4$ yr, roughly consistent with the dynamical age of the soft diffuse plasma ($\sim 2 \times 10^4$ yr). The X-ray emission from CXOU J171419.8–383023 is extended by ~ 0.05 (Aharonian et al. 2008) ($\sim 9 \text{ pc}$ at the distance of 10 kpc), consistent with those of middle-aged PWNe with characteristic ages of $\sim 10^3-10^4$ yr ($\sim 2-10 \text{ pc}$, Bamba et al. 2010). Thus many pieces of circumstantial evidence for PWN have been accumulating so far. However, no pulsation has been found from CXOU J171419.8–383023. We encourage deep pulsation search for the PWN candidate.

We would like to express our thanks to all of the Suzaku team. This work was supported by the Japan Society for the Promotion of Science (JSPS); the Grant-in-Aid for Scientific Research (C) 21540234 (SY), 24540232 (SY), and 24540229 (KK), Challenging Exploratory Research program 20654019 (KK), and Specially Promoted Research 23000004 (KK).

References

- Aharonian, F., et al. 2008, *A&A*, 490, 685
- Anders, E., & Grevesse, N. 1989, *Geochim. Cosmochim. Acta*, 53, 197
- Bamba, A., Anada, T., Dotani, T., Mori, K., Yamazaki, R., Ebisawa, K., & Vink, J. 2010, *ApJ*, 719, L116
- Castro, D., & Slane, P. 2010, *ApJ*, 717, 372
- Clark, D. H., Caswell, J. L., & Green, A. J. 1975, *Australian Journal of Physics Astrophysical Supplement*, Sept., 1
- Dame, T. M., Hartmann, D., & Thaddeus, P. 2001, *ApJ*, 547, 792
- Dickey, J. M., & Lockman, F. J. 1990, *ARA&A*, 28, 215
- Frail, D. A., Goss, W. M., Reynoso, E. M., Giacani, E. B., Green, A. J., & Otrupcek, R. 1996, *AJ*, 111, 1651
- Green, D. A. 2009, *Bull. Astr. Soc. India*, 37, 45⁴
- Kalberla, P. M. W., Burton, W. B., Hartmann, Dap, Arnal, E. M., Bajaja, E., Morras, R., & Pöppel, W. G. L. 2005, *ã*, 440, 775

⁴ <http://www.mrao.cam.ac.uk/surveys/snr/s/>

- Hyodo, Y., Tsujimoto, M., Hamaguchi, K., Koyama, K., Kitamoto, S., Maeda, Y., Tsuboi, Y., & Ezoe, Y. 2008, PASJ, 60, S85
- Kaastra, J. S., Mewe, R., & Nieuwenhuijzen, H. 1996, UV and X-ray Spectroscopy of Astrophysical and Laboratory Plasmas, ed. K. Yamashita and T. Watanabe (Universal Academy Press, Tokyo), p.411
- Kargaltsev, O., & Pavlov, G. G. 2008, 40 years of Pulsars: Millisecond Pulsars, Magnetars and More, AIP conference proceedings Vol. 983, p.171
- Koyama, K., et al. 2007, PASJ, 59, S23
- Mattana, F., et al. 2009, ApJ, 694, 12
- Mitsuda, K., et al. 2007, PASJ, 59, S1
- Morrison, R., & McCammon, D. 1983, ApJ, 270, 119
- Nakajima, H., et al. 2008, PASJ, 60, S1
- Ohnishi, T., Koyama, K., Tsuru, T. G., Masai, K., Yamaguchi, H., & Ozawa, M. 2011, PASJ, 63, 527
- Ozawa, M., Koyama, K., Yamaguchi, H., Masai, K., & Tamagawa, T. 2009, ApJ, 706, L71
- Possenti, A., Cerutti, R., Colpi, M., & Mereghetti, S. 2002, A&A, 387, 993
- Reynoso, E. M., & Mangum, J. G. 2000, ApJ, 545, 874
- Sawada, M., & Koyama, K., 2012, PASJ, 64, 81
- Serlemitsos, P., et al. 2007, PASJ, 59, S9
- Sezer, A., Gök, F., Hudaverdi, M., & Ecran, E. N. 2011, MNRAS, 417, 1387
- Tawa, N., et al. 2008, PASJ, 60, S11
- Tian, W. W., & Leahy, D. A. 2012, MNRAS, 421, 2593
- Uchida, H., et al. 2012, PASJ, 64, 141
- Uchiyama, H., et al. 2009, PASJ, 61, S9
- Whiteoak, J. B. Z., & Green A. J. 1996, A&AS, 118, 329
- Yamaguchi, H., Ozawa, M., Koyama, K., Masai, K., Hiraga, J., Ozaki, M., & Yonetoku, D. 2009, ApJ, 705, L6
- Yamaguchi, H., Ozawa, M., & Ohnishi, T. 2012, Adv. Sp. Res., 49, 451
- Yamauchi, S., et al. 2002, Proc. of IAU 8th Asian-Pacific Regional Meeting Vol.II, ed. S. Ikeuchi et al. (Tokyo: Astronomical Society of Japan), 81
- Yamauchi, S., Ueno, M., Koyama, K., & Bamba, A. 2008, PASJ, 60, 1143
- Yamauchi, S., Nobukawa, M., Koyama, K., & Yonemori, M. 2013, PASJ, 65, 6